Morphology Development of Mesoporous Materials: a Colloidal Phase Separation Mechanism

Chengzhong Yu, Jie Fan, Bozhi Tian, and Dongyuan Zhao*

Department of Chemistry and Shanghai Key Laboratory of Molecular Catalysis and Innovative Materials, Fudan University 200433, P. R. China

Received October 14, 2003. Revised Manuscript Received December 8, 2003

Synthetic conditions such as temperature, stirring rate, ionic strength, acidity, and reactant ratios that affect the mesostructures and macrostructures of mesoporous materials have been extensively studied in the nonionic block copolymer templating system. Highly ordered SBA-15 materials with ∼100% rodlike morphologies (∼1−2 μm long) have been obtained in the presence of inorganic salts. Synthesis conditions such as low temperature, low acidity, and low ionic strength that increase the induction time give rise to the morphologies of mesoporous silica with increased curvatures. The particle growth process of rodlike SBA-15 materials from solutions has been examined by directly observing the morphologies of particles as a function of time. A colloidal phase separation mechanism (CPSM) for the formation of mesoporous materials is proposed. It is suggested that the formation process of mesoporous materials involves three stages: (1) cooperative self-assembly of inorganic/organic composites; (2) formation of a new crystal-like phase rich in aggregates of block copolymer/silica species; and (3) phase separation of this liquid crystal-like phase from the solution and further growth of solid mesostructures driven by further condensation of silica species. The morphologies of mesoporous materials are developed after the phase separation stage and influenced by the competition mainly between the free energy of mesostructure self-assembly (ΔG) and the colloidal surface free energy (F), as well as other interactions such as the shearing force. When the phase separation stage occurs early, ΔG is dominant and the macrostructure of mesoporous materials is developed together with the formation of mesostructure; therefore, mesoporous materials with crystal-like morphologies can be generated. The role of inorganic salts is well explained based on the CPSM by taking into account the colloidal interaction enhanced by inorganic salts. Cubic ($Im\bar{3}m$) mesoporous single crystals have been obtained with exclusively rhombdodecahedron shapes (1−2 μm in size). Ultrathin microtoming TEM measurements confirm that such polyhedral particles are perfect single crystals. The different influences of hydrothermal treatments upon the mesostructures and macrostructures have been discussed in the hexagonal and cubic synthesis systems. By employing the CPSM, hexagonal mesoporous single crystals have been obtained in the absence of inorganic salts; the size limitation (∼1−2 μm) of mesoporous single crystals has also been discussed. Such understandings may be useful in the fabrication of mesoporous materials with well-defined, crystal-like morphologies.

Introduction

Since the pioneering reports by Mobil and Japanese scientists,[1−3] surfactant templated mesostructured materials have attracted much attention because of their emerging applications in catalysis, adsorption, sensors, and separations.[4−6] Recently, poly(ethylene oxide) (PEO) nonionic surfactants or block copolymers have been studied extensively as structure-directing agents in the synthesis of highly ordered mesostructured materials.[7,8] Fabrication of mesoporous materials with controllable morphologies has been one of the main subjects in this rapidly developing research field. Mesoporous materials in the form of films,[9,10] monoliths,[11,12] spheres,[13,14]

* To whom correspondence should be addressed. E-mail: dyzhao@fudan.edu.cn.

(1) Kresge, C. T.; Leonowicz, M. E.; Roth, W. J.; Vartuli, J. C.; Beck, J. S. *Nature* **1992**, *359*, 710.
(2) Beck, J. S.; Vartuli, J. C.; Roth, W. J.; Leonowicz, M. E.; Kresge, C. T.; Schmitt, K. D.; Chu, C. T. W.; Olson, D. H.; Sheppard, E. W.; McCullen, S. B.; Higgins, J. B.; Schlenker, J. L. *J. Am. Chem. Soc.* **1992**, *114*, 10834.
(3) Yanagisawa, T.; Shimizu, T.; Kuroda, K.; Kato, C. *Bull. Chem. Soc. Jpn.* **1990**, *63*, 988.
(4) Ying, J. Y.; Mehnert, C. P.; Wong, M. S. *Angew. Chem., Int. Ed.* **1999**, *38*, 56.
(5) Davis, M. E. *Nature* **2002**, *417*, 813.
(6) Stein, A. *Adv. Mater.* **2003**, *15*, 763.
(7) Zhao, D. Y.; Feng, J. L.; Huo, Q. S.; Melosh, N.; Fredrickson, G. H.; Chmelka, B. F.; Stucky, G. D. *Science* **1998**, *279*, 548.
(8) Zhao, D. Y.; Huo, Q. S.; Feng, J. L.; Chmelka, B. F.; Stucky, G. D. *J. Am. Chem. Soc.* **1998**, *120*, 6024.
(9) Zhao, D.; Yang, P.; Melosh, N.; Feng, J.; Chmelka, B. F.; Stucky, G. D. *Adv. Mater.* **1998**, *10*, 1380.
(10) Miyata, H.; Noma, T.; Watanabe, M.; Kuroda, K. *Chem. Mater.* **2002**, *14*, 766.
(11) Feng, P. Y.; Bu, X. H.; Stucky, G. D.; Pine, D. J. *J. Am. Chem. Soc.* **2000**, *122*, 994.
(12) Yang, H. F.; Shi, Q. H.; Tian, B. Z.; Xie, S. H.; Zhang, F. Q.; Yan, Y.; Tu, B.; Zhao, D. Y. *Chem. Mater.* **2003**, *15*, 536.
(13) Zhao, D. Y.; Sun, J. Y.; Li, Q. Z.; Stucky, G. D. *Chem. Mater.* **2000**, *12*, 275.

10.1021/cm035011g CCC: $27.50
Published on Web 02/11/2004

fibers,[13,15] rodlike powders,[14,16,17] and crystals[18] have been obtained in block copolymer templating systems. It is important to design the morphology of mesoporous materials as well as the mesostructure for desired applications. For example, mesoporous films may be used in membrane separation[19] and gas sensing.[20] For the particles, mesoporous spheres may be utilized in high-performance liquid chromatography as a stationary phase,[21] while rodlike SBA-15 materials possess bioimmobilization abilities for lysozymes much improved over that of conventional SBA-15 materials.[22] However, although several mechanisms have been proposed for the formation of mesostructures,[1,8,23−32] few mechanisms have been proposed for the development of macrostructures, especially for particles grown from aqueous solutions with dilute surfactant concentrations.

Ozin and co-workers have studied the morphosynthesis of self-assembled mesostructured materials, mostly dealing with curved shapes that resemble those of minimal surfaces rather than polyhedral crystal habits.[33] Chan et al. proposed a simple phase separation mechanism based on their observation of the particle development of MCM-41 materials.[34] Until now, studies of the formation mechanisms for mesostructured single crystals templated either by ionic surfactants[35−39] or by nonionic block copolymers[18] has not been reported.

We have studied the effect of inorganic salts used in the synthesis of mesostructured materials in the presence of block copolymer templates.[17,18,40,41] Highly ordered rodlike (∼1−2 μm long) hexagonal ($p6m$) mesostructured SBA-15 materials were obtained in the presence of inorganic salts such as KCl and further employed as the templates to synthesize rodlike mesoporous carbon.[17] Cubic ($Im\bar{3}m$) mesostructured single crystals with exclusively uniform rhombdodecahedron shapes (1−2 μm) were also synthesized using a commercial nonionic block copolymer as a template under acidic conditions.[18] It should be noted that in the above two cases, the yield of desired morphologies is ∼100%; therefore, it was possible to systematically study the morphology development as a function of time. Moreover, recent results in our lab have indicated that such rodlike SBA-15 materials are better candidates for immobilization of enzymes than conventional SBA-15 materials.[22] It is therefore theoretically and practically important to study in detail how these rodlike particles are grown from solutions.

In this paper the effects of synthetic conditions such as temperature, stirring rate, ionic strength, acidity, and reactant ratios upon the macrostructures of mesoporous materials have been carefully examined. The particle growth process for rodlike SBA-15 materials from dilute solutions was studied by directly observing the morphologies of particles as a function of time. A colloidal phase separation mechanism (CPSM) for the formation of mesostructured materials is proposed to describe the development of macrostructures. The different influences of hydrothermal treatments upon the mesostructures and macrostructures have been compared in the hexagonal and cubic synthesis systems. By employing the CPSM, hexagonal mesostructured single crystals have been obtained in the absence of inorganic salts. The size limitation of mesoporous single crystals has also been discussed. Understanding these synthesis parameters can be expected to be useful in the fabrication of mesostructured materials with well-defined, crystal-like morphologies.

Experimental Section

Synthesis. PEO nonionic block copolymers with poly(propylene oxides) (PPO) hydrophobic moieties P123 ($EO_{20}PO_{70}EO_{20}$) and F108 ($EO_{132}PO_{50}EO_{132}$) were received as gifts from BASF. All commercial chemicals were used without purification. Tetraethyl orthosilicate (TEOS) or tetramethyl orthosilicate (TMOS) were employed as the silica source in the present study.

For a typical synthesis of rodlike SBA-15 materials, 2.0 g (0.4 mmol) of P123 and 2.2 g (30 mmol) of potassium chloride were dissolved in 60 mL of 2.0 M HCl at 38 °C. To this solution, 4.2 g (20 mmol) of TEOS was added under vigorous stirring. The final reactant molar composition was 0.02:1.5:6:166:1 P123/KCl/HCl/H_2O/TEOS. After stirring for 8 min, the mixture was kept in static condition at the same temperature for 1 day, then the mixture was transferred into an autoclave and heated at 100 °C for another 24 h. The solid products were collected by filtration, washed with water, and dried at room temperature in air. The resulted powders were calcined at 550 °C for 4 h to remove the templates and obtain mesoporous silica materials.

(14) Boissiere, C.; Larbot, A.; van der Lee, A.; Kooyman, P. J.; Prouzet, E. *Chem. Mater.* **2000**, *12*, 2902.
(15) Yang, P. D.; Zhao, D. Y.; Chmelka, B. F.; Stucky, G. D. *Chem. Mater.* **1998**, *10*, 2033.
(16) Schmidt-Winkel, P.; Yang, P. D.; Margolese, D. I.; Chmelka, B. F.; Stucky, G. D. *Adv. Mater.* **1999**, *11*, 303.
(17) Yu, C. Z.; Fan, J.; Tian, B. Z.; Zhao, D. Y.; Stucky, G. D. *Adv. Mater.* **2002**, *14*, 1742.
(18) Yu, C. Z.; Tian, B. Z.; Fan, J.; Stucky, G. D.; Zhao, D. Y. *J. Am. Chem. Soc.* **2002**, *124*, 4556.
(19) Boissiere, C.; Martines, M. A. U.; Kooyman, P. J.; de Kruijff, T. R.; Larbot, A.; Prouzet, E. *Chem. Mater.* **2003**, *15*, 460.
(20) Yamada, T.; Zhou, H. S.; Uchida, H.; Tomita, M.; Ueno, Y.; Ichino, T.; Honma, I.; Asai, K.; Katsube, T. *Adv. Mater.* **2002**, *14*, 812.
(21) Boissiere, C.; Kummel, M.; Persin, M.; Larbot, A.; Prouzet, E. *Adv. Funct. Mater.* **2001**, *11*, 129.
(22) Fan, J.; Lei, J.; Wang, L. M.; Yu, C. Z.; Tu, B.; Zhao, D. Y. *Chem. Commun.* **2003**, 2140.
(23) Huo, Q. S.; Margolese, D. I.; Ciesla, U.; Feng, P. Y.; Gier, T. E.; Sieger, P.; Leon, R.; Petroff, P. M.; Schuth, F.; Stucky, G. D. *Nature* **1994**, *368*, 317.
(24) Huo, Q. S.; Margolese, D. I.; Ciesla, U.; Demuth, D. G.; Feng, P. Y.; Gier, T. E.; Sieger, P.; Firouzi, A.; Chmelka, B. F.; Schuth, F.; Stucky, G. D. *Chem. Mater.* **1994**, *6*, 1176.
(25) Tanev, P. T.; Pinnavaia, T. J. *Science* **1995**, *267*, 865.
(26) Bagshaw, S. A.; Prouzet, E.; Pinnavaia, T. J. *Science* **1995**, *269*, 1242.
(27) Attard, G. S.; Glyde, J. C.; Goltner, C. G. *Nature* **1995**, *378*, 366.
(28) Antonelli, D. M.; Ying, J. Y. *Angew. Chem. Int. Ed. Engl.* **1996**, *35*, 426.
(29) Brinker, C. J.; Lu, Y. F.; Sellinger, A.; Fan, H. Y. *Adv. Mater.* **1999**, *11*, 579.
(30) Patarin, J.; Lebeau, B.; Zana, R. *Curr. Opin. Colloid Interface Sci.* **2002**, *7*, 107.
(31) Zhang, J. Y.; Carl, P. J.; Zimmermann, H.; Goldfarb, D. *J. Phys. Chem. B* **2002**, *106*, 5382.
(32) Ruthstein, S.; Frydman, V.; Kababya, S.; Landau, M.; Goldfarb, D. *J. Phys. Chem. B* **2003**, *107*, 1739.
(33) Ozin, G. A. *Can. J. Chem.* **1999**, *77*, 2001.
(34) Chan, H. B. S.; Budd, P. M.; Naylor, T. D. *J. Mater. Chem.* **2001**, *11*, 951.
(35) Kim, J. M.; Kim, S. K.; Ryoo, R. *Chem. Commun.* **1998**, 259.
(36) Guan, S.; Inagaki, S.; Ohsuna, T.; Terasaki, O. *J. Am. Chem. Soc.* **2000**, *122*, 5660.
(37) Sayari, A. *J. Am. Chem. Soc.* **2000**, *122*, 6504.
(38) Che, S.; Sakamoto, Y.; Terasaki, O.; Tatsumi, T. *Chem. Mater.* **2001**, *13*, 2237.
(39) Trikalitis, P. N.; Rangan, K. K.; Bakas, T.; Kanatzidis, M. G. *J. Am. Chem. Soc.* **2002**, *124*, 12255.
(40) Yu, C. Z.; Tian, B. Z.; Fan, J.; Stucky, G. D.; Zhao, D. Y. *Chem. Commun.* **2001**, 2726.
(41) Yu, C. Z.; Fan, J.; Zhao, D. Y. *Acta Chim. Sin.* **2002**, *60*, 1357.

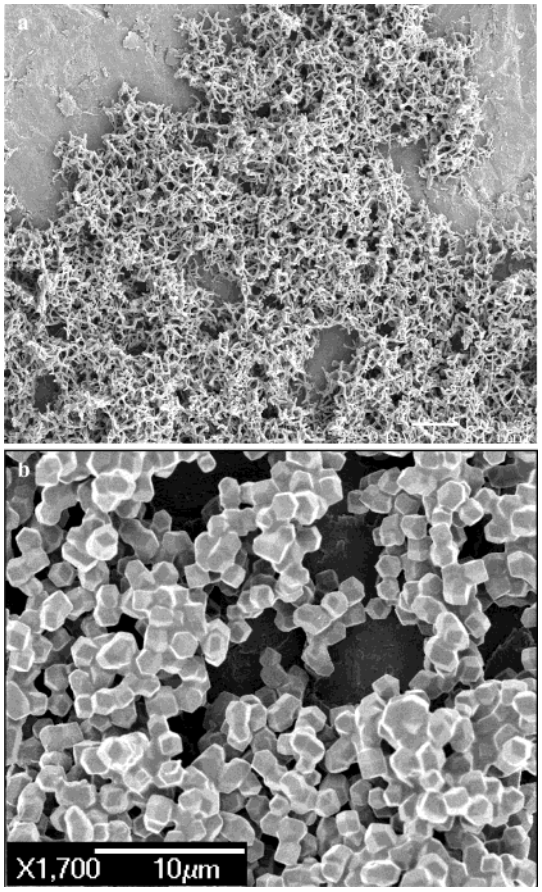

Figure 1. SEM images in large scale of (a) rodlike SBA-15 and (b) cubic mesoporous silica crystals synthesized by using P123 and F108 as the templates, respectively.

In a typical synthesis of cubic mesostructured silica single crystals, 2 g of triblock copolymer F108 and 5.24 g of K_2SO_4 were dissolved in 60 g of 2 mol/L HCl at 40 °C. To this solution, 4.2 g of TEOS was added under stirring for 15 min and then the reaction was continued under static conditions for 24 h at 40 °C. The final reactant molar composition was 0.007:1.5:6:166:1 F108/K_2SO_4/HCl/H_2O/TEOS. The solid products were collected by filtration, washed with hot water, and dried at room temperature in air. The resulting powders were calcined at 400 °C for 4 h to remove the templates. Details of hydrothermal treatments of the resultant as-synthesized samples are described in Results and Discussion.

Platelike SBA-15 was synthesized by using TMOS as a silica source at 303 K under static condition. In a typical synthesis, 2.0 g (0.34 mmol) of P123 was dissolved in 60 g (120 mmol) of 2.0 M HCl at 30 °C. To this solution, 3.3 g (22 mmol) of TMOS was added under vigorous stirring. The final reactants molar composition was 0.015:5.5:150:1 P123/HCl/H_2O/TEOS. After the mixture was stirred for 6 min, it was kept in static condition at the same temperature for 1 day, then transferred into an autoclave and heated at 100 °C for another 24 h. The solid products were collected by filtration and dried at room temperature in air. The resulted powders were calcined at 550 °C for 4 h to obtain mesoporous silica materials.

Characterization. The powder X-ray diffraction (XRD) patterns were collected on a Scintag PADX diffractometer using Cu Ka radiation. Scanning electron microscopy (SEM) images were obtained with a JEOL 6300-F field emission microscope using 3.0-kV acceleration voltages. Transmission electron microscopy (TEM) micrographs were obtained with a JEOL 2000 operating at 200 kV. The nitrogen sorption isotherms were measured at −196 °C by using a Micromeritics ASAP 2000 system. The samples were degassed at 180 °C overnight on a vacuum line. Thermogravimetry analysis (TGA) was performed on a Rigaku PTC-10A analyzer with a temperature rate of 10 °C/min in air.

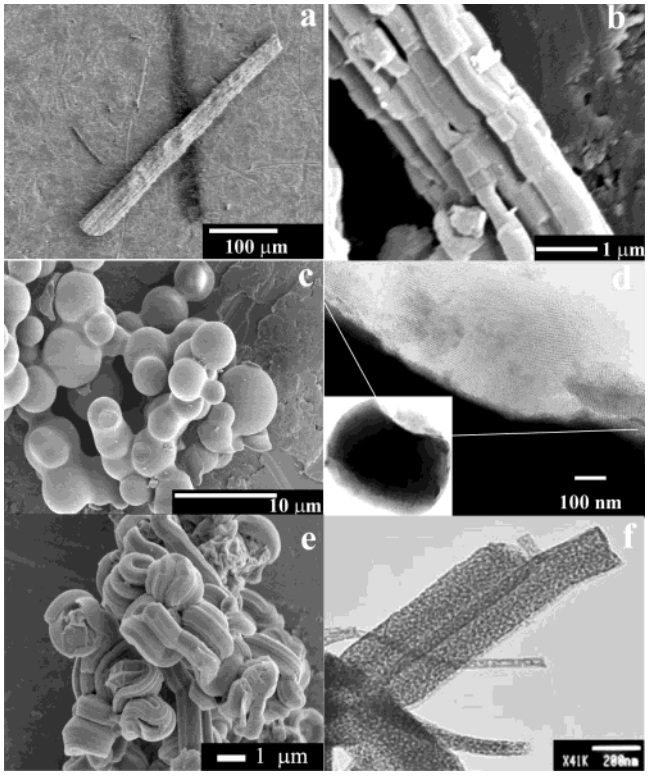

Figure 2. SEM images of as-synthesized SBA-15 materials synthesized at the same reactant molar ratio of 0.02:1.5:6:166:1 P123/KCl/HCl/H_2O/TEOS: (a) at 38 °C under stirring condition; (b) at high magnification of (a); (c) at 20 °C under static condition. TEM images (d) of calcined SBA-15 materials synthesized at 20 °C under static condition, inset of (d) shows a spherical morphology at low magnification. SEM image (e) of as-synthesized SBA-15 materials synthesized at 30 °C under static condition. TEM images (f) of as-synthesized SBA-15 materials synthesized at 45 °C under static condition.

Results and Discussion

Synthesis of Rodlike SBA-15. At 38 °C and a reactant molar ratio of 0.02:1.5:6:166:1 P123/KCl/HCl/H_2O/TEOS, SBA-15 materials with ∼100% rodlike morphology can be obtained, as confirmed by SEM images observed in large scale (Figure 1a). The induction time from addition of TEOS to the occurring of milky-white precipitates in solution is found to be ∼15 min and not dependent on stirring condition. It is important that after adding TEOS with stirring for 8 min to generate a homogeneous solution, the mixture must be kept in static condition to yield the final rodlike morphology (referred to as static condition hereafter although a period of time for stirring is needed at the beginning). Synthesis parameters such as stirring rate, temperature, ionic strength, acidity, and reactant ratio have a strong influence upon the morphologies of SBA-15 materials. With continuous stirring at constant temperature using the same reactant molar ratio as in the synthesis of rodlike SBA-15 materials, fiberlike morphologies SBA-15 with lengths as much as several hundreds of micrometers are observed (Figure 2a). It is interesting to note that such fiberlike SBA-15 materials are composed of "basic" rodlike units (∼1−2 μm

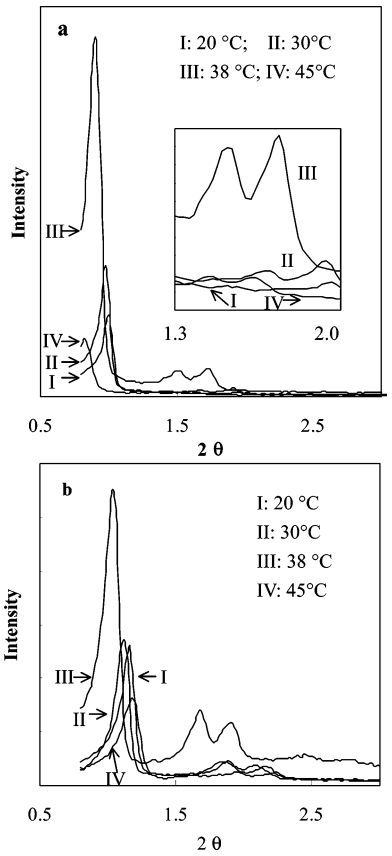

Figure 3. XRD patterns of (a) as-synthesized and (b) calcined SBA-15 materials synthesized at the reactant molar ratio (0.02:1.5:6:166:1 P123/KCl/HCl/H_2O/TEOS) under static condition at 20, 30, 38, and 45 °C.

long), coupled along the long axis to give the fibrous morphologies (Figure 2b).

When the reactant molar ratio is kept at 0.02:1.5:6:166:1 P123/KCl/HCl/H_2O/TEOS, SBA-15 materials are synthesized at 20, 30, 38, and 45 °C under static condition. XRD profiles of both as-synthesized and calcined SBA-15 materials synthesized at different temperatures show similar patterns (Figure 3), which can be attributed to a hexagonal symmetry ($p6m$),[7] suggesting that the variation of temperature (20−45 °C) has little influence on the mesostructure of SBA-15 materials. The *d*-spacing of the first diffraction peak (10) is calculated to be 8.82, 9.19, 9.80, and 10.5 nm for as-synthesized samples and 7.61, 7.88, 8.48, and 7.48 for calcined materials synthesized at 20, 30, 38, and 45 °C, respectively. With increasing temperature (20 to 38 °C), the intensity of the first diffraction peak (10) increases particularly in the as-synthesized samples (Figure 3a) and the value of the *d*-spacing increases (in both as-synthesized and calcined samples). In the XRD patterns of SBA-15 materials synthesized at 45 °C, it is abnormal that the intensity of the first diffraction peak is lower than that for SBA-15 synthesized at 38 °C. Moreover, the *d*-spacing of the first diffraction peak in the as-synthesized sample synthesized at 45 °C is larger than that synthesized at 38 °C, but the *d*-spacing of the first diffraction peak in the calcined sample synthesized at 45 °C is smaller than that of the calcined sample synthesized at 20 °C. Furthermore, the full width at half-maximum (fwhm) of the first diffraction peak for calcined samples synthesized at 45 °C is ∼1.5 times broader than that at 38 °C. Such observations will be further discussed in the next paragraph.

The macrostructures of SBA-15 materials show a substantial dependence on temperature. At 20 °C, mostly spherical shapes (2−8 μm diameter) are observed (Figure 2c). TEM measurements further confirm the spherical morphology (inset of Figure 2d), The observed stripe-like patterns at thin sections of spheres are in accordance with the hexagonal structure confirmed by XRD results (Figure 2d). At 30 °C, rodlike morphologies with both straight and curved shapes are obtained (Figure 2e). Many stripes parallel to the long axis of the rods are observed, in accordance with the TEM results we reported before[17] and the intrinsic hexagonal mesostructures of such rodlike materials. Such stripes cannot be observed in spherical SBA-15 materials synthesized at relatively low temperature (20 °C). At 38 °C, ∼100% straight rodlike morphology (1−2 μm long) is obtained (Figure 1a). When the temperature is further increased to 45 °C, the rodlike morphology is still retained in resultant products; however, careful TEM measurements show that an impurity mesophase (Figure 2f) coexists with the hexagonal mesostructured phase. This observation is in accordance with the phase diagram of P123,[42] in which a mixed-phase region occurs when the temperature is raised from the hexagonal region to above ∼ 45 °C. We propose that the synthesis temperature of 45 °C should be the upper temperature limit of the hexagonal region in SBA-15 synthesis phase diagram (ionic strength should be considered). SBA-15 materials synthesized at the boundary temperature (45 °C) between the hexagonal and mixed phase region have less stable hexagonal structures than at relatively low temperatures (20−38 °C, within hexagonal region), which can also be observed by the abnormal XRD patterns (see discussion in previous paragraph).

At 38 °C, other synthesis factors are examined by tuning only one factor in the reactant composition synthesis space (2:2.2:60:4.2 P123/KCl/2 M HCl/TEOS). As expected, the variation in reactant composition and molar ratio is also found to be important to the final morphology. Increasing the silica/P123 ratio (from 4.2:2 to 6.3:2, weight ratio) leads to a spherical morphology (similar to that shown in Figure 2c). When the acidity is decreased (0.5 M HCl is used instead of 2 M HCl), a curved rodlike morphology similar to that shown in Figure 2e is observed. When the concentration of KCl in the reactant composition is decreased from 0.5 to 0.25 M, both straight and curved rodlike morphologies are obtained. On the other hand, increasing the concentration of KCl (from 0.5 to 1.0 M) gives rise to straight rodlike SBA-15 materials. Other inorganic salts such as Na_2SO_4 and K_2SO_4 also produce straight rodlike morphology at concentrations higher than 0.25 M. However, curved rodlike to spherical shaped SBA-15 materials are formed when the concentration of Na_2SO_4 is decreased (0.25 to 0.05 M). In our experiments, the morphology of SBA-15 materials is much more dependent on the ionic strength than the type of cations or anions in the inorganic salts.[43,44] It may be concluded

(42) Wanka, G.; Hoffmann, H.; Ulbricht, W. *Macromolecules* **1994**, *27*, 7, 4145.
(43) Leontidis, E. *Curr. Opin. Colloid Interface Sci.* **2002**, *7*, 81.
(44) Che, S. N.; Lim, S. Y.; Kaneda, M.; Yoshitake, H.; Terasaki, O.; Tatsumi, T. *J. Am. Chem. Soc.* **2002**, *124*, 13962.

that factors that shorten the induction time[8] such as relatively high temperature, high concentration of acid, and high ionic strength, may favor the formation of straight rodlike SBA-15 materials. On the other hand, experimental conditions that increase the induction time may increase the curvature of the resulting morphology. For example, the induction time for the synthesis of SBA-15 materials with the same reactant ratio (0.02: 1.5:6:166:1 P123/KCl/HCl/H_2O/TEOS) at 45, 38, 30, and 20 °C is estimated to be 9, 15, 24, and 35 min, respectively; and the morphology changes from straight rodlike (smallest curvature) to curved rodlike and finally to spherical morphology (possessing the largest curvature).

Growth of Rodlike SBA-15. At optimum condition (static condition, 38 °C, and reactant molar ratio of 0.02: 1.5:6:166:1 P123/KCl/HCl/H_2O/TEOS) SBA-15 materials with ∼100% rodlike morphology have been synthesized (Figure 1a). Because the final morphology is uniform, it offers us an opportunity to study how these rodlike particles grow from solutions. This process was monitored by direct SEM observations of samples separated at different times after the precipitation occurred in solutions. The precipitates that formed after 2 min were removed by direct filtration, then washed with water and ethanol to remove the surfactants and the unreacted silica species in solution in order to avoid continuous particle growth during this time interval.

By using 0.5 mol/L KCl at 38 °C, the white precipitates can be seen in ∼15 min after the addition of TEOS. Attempts to separate the solids by filtration immediately after the precipitation occurred were unsuccessful, suggesting that the particles formed at this stage are too small. If ethanol is used to wash the solids, the products disappear in solutions, suggesting that either the chemical process of self-assembly/silica condensation is quite reversible at this stage, or the sizes of the particles are less than 100 nm. Indeed, SEM images of the samples isolated ∼2 min after precipitation show amorphous aggregates with diameters smaller than 100 nm (Figure 4a). However, after 5 min, spheres with diameters from ∼50 to ∼100 nm can be seen (Figure 4b). Some spheres are joined together and elongating in one direction (Figure 4c). TEM observations prove that these spheres contain wormlike mesoporous structures; no hexagonal order is found (Figure 4d). After 20 min, the rods with straight and curved shapes and some large spheres are observed (Figure 4e). After 1 h, only straight rods are observed (Figure 4f), and this morphology is retained during further condensation of silica species and hydrothermal treatment. Actually there is a time interval from taking the specimen to SEM observation, and the sample treating methods necessary for SEM observation may change the morphology more or less, thus the whole process is not observed strictly in situ; however, the trend of the particle development is obvious: the straight rods (1−2 μm long) with finally *p6m* symmetry are generated from poorly ordered colloidal spheres (smaller than ∼100 nm diameter).

Colloidal Phase Separation Mechanism (CPSM). On the basis of the results above, we propose a mechanism for mesoporous materials precipitated from solutions taking into account both the mesostructure and macrostructure formation (Figure 5). The process includes the following three stages. The first stage is the *cooperative assembly* at the molecular level to form surfactant/silica composite aggregates. Charge density matching between the surfactant headgroups and hydrolyzed inorganic oligomers is important at this stage; details of this stage have been discussed extensively[23,24] and therefore are less considered in the following discussion.

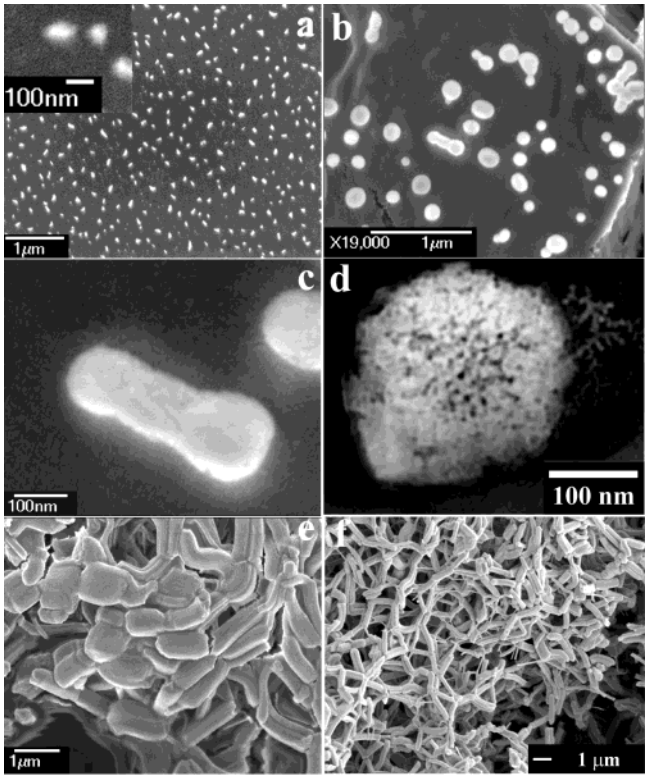

Figure 4. SEM images (a), (b) (c), (e), and (f) of samples prepared with 0.5 mol/L KCl at 38 °C but separated at different times after precipitation: (a) 2 min; (b) 5min; (c) at high magnification of (b); (e), 20 min; and (f) 1 h. (d) TEM images of samples separated after 5 min.

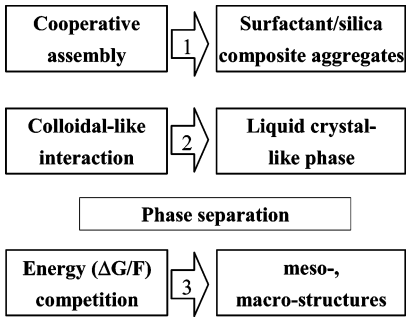

Figure 5. Schematic drawing of colloidal phase separation mechanism.

The second stage is *colloidal-like interaction* of these surfactant/silica aggregate composites. Further condensation of silica species leads to interconnection of the composite aggregates to give a new liquid crystal-like phase made up of the block copolymer/silica species. As the silica species further condense, the new liquid phase grows denser with time and finally separates from the water phase. The time when this liquid/liquid phase separation occurs may be assigned to when the precipitate is first observed in the solution. The spherical shapes that we observed shortly after the phase separa-

tion (<5 min, Figure 4b) support this liquid/liquid phase separation mechanism, as a separated liquid phase will take the shape of spheres to minimize the surface free energy (F); moreover, such spheres with small diameters should grow larger in order to minimize the surface area and therefore F. It should be noted that this newly formed liquid phase can be regarded as the precursor of the final highly ordered liquid crystal phase (so-called liquid crystal-like phase), because at the time the liquid/liquid phase separates and a short period of time after that point, no ordered liquid crystal structures can be observed in the products (Figure 4d).

The third stage is multiphase *energy competition* after the phase separation. At this stage the mesostructure assembly is still under way, and the separated liquid crystal-like phase is further growing into the final solid mesostructure. Although the free energy of the mesophase formation (ΔG) is responsible for the final mesostructure, the competition between ΔG and the surface free energy (F) of this liquid crystal-like phase determines the morphology of final mesoporous materials.

The formation of mesostructures involves the assembly of surfactant/inorganic composite aggregates (in dilute solutions) into cross-linked inorganic/organic frameworks with liquid crystal structures (in final solid products). The self-assembly ability of the surfactant and the further condensation of inorganic species should be considered for the whole chemical process. For the mesoporous silica synthesis systems with the same block copolymers under similar acidic condition, it is proposed that the time interval from addition of TEOS to phase separation (the induction time) may be used approximately to estimate the free energy change of the composite mesophase formation. ΔG becomes less negative with increasing time because the condensation of inorganic silica species is progressing with time. When the phase separation occurs early, ΔG is dominant in the synthesis system, so that the morphology of the particles is developed together with the formation of ordered mesostructures. The final particle morphology reflects the intrinsic liquid crystal structure (e.g., rodlike SBA-15 synthesized at optimum condition). On the other hand, if the phase separation occurs more slowly, F will have considerable influence upon the macrostructure because the morphology is developed by surface energy effects during transformation from liquid crystal-like phase to solid phase. With the increasing influence of F, a morphology with large curvature will be generated in order to minimize the surface energy (e.g., spherical SBA-15 synthesized at 20 °C).

CPSM may be used to re-interpret the effect of inorganic salts upon the morphology of mesoporous materials. In the case of P123 templated hexagonal mesoporous materials, it has been shown that the use of inorganic salts may result in straight rodlike morphologies.[14,16,17] However, the underlying reason has not been clearly explained, as the enhancement of $(S^0H^+)(X^-I^+)$ interaction[8] at molecular level by inorganic salts does not account for the formation of macrostructures with different shapes.

Viewing the surfactant/silica composite aggregates initially formed in dilute solution from a colloidal point of view, it is energetically unfavorable for these colloidal particles to approach each other because of electrostatic repulsion according to the well-known Derjaguin−Landau−Verwey−Overbeek (DLVO) theory.[45] When the ionic strength of the solution is increased, the energy barrier is decreased. Finally, at a certain high ionic strength, the aggregation of colloidal particles becomes energetically favorable (Figure 6). The observed contrast in induction time (~60/15 min) during the synthesis of SBA-15 without and with KCl (0.5 M) is in good accordance with the DLVO theory. Because the phase separation time is much shorter in the latter case, straight rodlike morphology with one-dimensional (1D) channels parallel to the long axis of rods is obtained, reflecting quite well the hexagonal structure of SBA-15 materials.

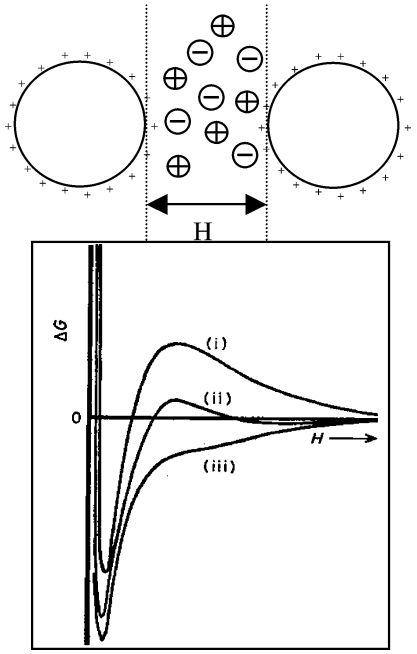

Figure 6. Total free energy difference ΔG between colloidal particles at infinite separation and at a separation distance H as a function of H at different ionic strengths: (i) < (ii) < (iii).

In addition to ΔG and F, other forces in solution such as shearing force induced by stirring should also be considered for the formation of macrostructures. Because the morphology is developed after the phase separation of the liquid crystal-like phase from water, such phase-separated liquid droplets are easily aligned along the direction of shearing force and further grow into fiberlike SBA-15 materials.

Synthesis of Cubic SBA-16 Single Crystals. At 40 °C and a final reactant molar composition of 0.007:1.5:6:166:1 F108/K_2SO_4/HCl/H_2O/TEOS under static conditions (referred to as optimum condition), highly ordered cubic ($Im\bar{3}m$) mesoporous single crystals with exclusively uniform rhombdodecahedron shapes (1−2 μm in size) have been obtained.[18] Figure 1b shows SEM images of as-synthesized crystals in large scale. To reveal the internal crystal structure, the specimen for TEM observation was prepared by ultrathin microtoming method. It is interesting to note that both square

(45) Everett, D. H. *Basic Principles of Colloid Science*; Royal Society of Chemistry Paperbacks; Royal Society of Chemistry: Cambridge, 1994.

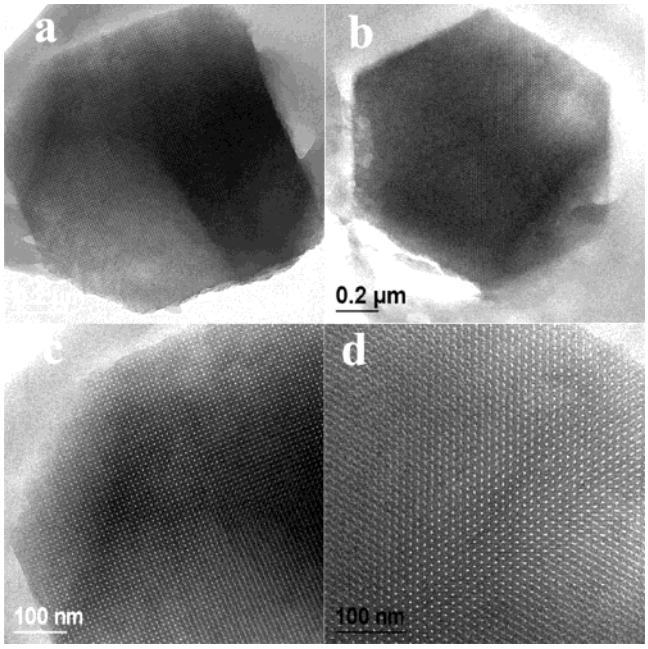

Figure 7. TEM images of cubic mesoporous single crystals prepared with 0.007:1.5:6:166:1 F108/K_2SO_4/HCl/H_2O/TEOS at 38 °C under static conditions: (a) along [100] direction; (b) along [111] direction; (c) and (d) high magnification images of (a) and (b), respectively. Samples for TEM observation were pretreated with ultrathin microtoming method.

and hexagon shapes are found under TEM observations (Figure 7, a and b, respectively), which correspond to the sections perpendicular to the 4-fold and 3-fold axis of such rhombdodecahedron crystals, respectively. More strikingly, only [100] and [111] patterns are observed in the entire range of squares and hexagons, respectively (Figure 7, c and d, respectively). In addition, the diagonal of the *bcc* unit cell is found to be parallel to the edge of the square (Figure 7a and c). In previous studies,[18] by directly observing the mesopore array of each crystal, it has been revealed that TEM images along only [110] direction is observed in each {110} crystal face, and the diagonal of the rectangular repeating unit is parallel to the crystal edge. All these data are in accordance with an ideal crystal model with bcc symmetry. It should be noted that such TEM images are obtained in view of the entire external crystal face as well as the sections of an entire particle, unambiguously confirming the single-crystal nature of such mesoporous materials.

Synthesis conditions may severely affect the morphology of mesoporous materials templated by F108 surfactants (Supporting Information (SI) Table 1). At optimum condition (SI Table 1, sample A), the induction time is observed to be ∼35 min and ∼100% crystals are obtained (Figure 1b). At the same reactant ratio but without salt (SI Table 1, sample B), the induction time is ∼3 h and amorphous silica structures are synthesized (XRD results, data not shown). The same concentration of Na_2SO_4 (0.5 M) instead of K_2SO_4 also gives rise to exclusively rhombdodecahedron morphologies (1−2 μm in size, SI Table 1, sample C), the induction time (∼31 min) is also similar to that observed in optimum synthesis conditions. However, the use of 1 M KCl instead of 0.5 M K_2SO_4 results in a fast induction time of ∼27 min (SI Table 1, sample D) and produces

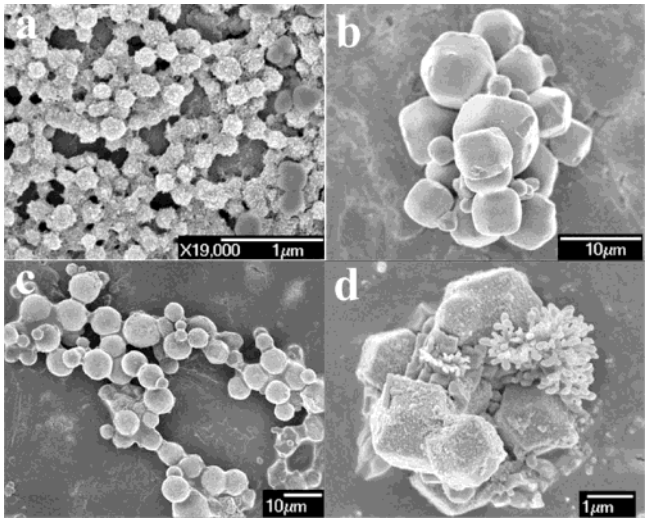

Figure 8. SEM images of cubic mesoporous materials synthesized with F108 template at 38 °C under static condition: (a) with 1.0 M KCl; (b) with 0.5 M HCl; (c) with TEOS/F108 = 6.2/2 (weight ratio); and (d) at optimum condition and hydrothermal treated directly without filtration.

spherical particles ∼150 nm in diameter (Figure 8a); even when 0.5 M KCl is used and the induction time is similar to that in optimum conditions (SI Table 1, sample E), only spherical morphologies (100−1000 nm diameters) are observed, indicating that anions are important in the synthesis and morphology control of cubic mesoporous crystals.[43,44] When 0.5 M HCl is utilized instead of 2 M HCl (SI Table 1, sample F), the induction time is as long as 2.5 h and the resultant particles possess sizes not uniform in diameter (1−10 μm). The morphologies of such particles clearly show transition from polyhedral to spherical shapes as a function of induction time (Figure 8b). Such observation may be readily explained in the CPSM: the decreasing influence of ΔG with increasing induction time may lead to particle morphologies with increasing curvature (F plays more important roles). In the range of temperatures under study (SI Table 1, samples A, G, H, and I; 40, 35, 30, and 47 °C, respectively), syntheses at 40 and 35 °C all produce ∼100% crystal morphologies; whereas relatively low or high-temperatures all give rise to mixed morphologies (crystals and spheres). Such mixed morphologies are also observed in syntheses in which an increased silica/surfactant ratio is employed (SI Table 1, sample J, and Figure 8c). The utilization of 1 M H_2SO_4 as acid source instead of 2 M HCl produces all spherical morphologies, possibly due to the increasing concentration of SO_4^{2-} in solutions (SI Table 1, sample K). These observations show that the temperature, reactant ratio, and acid source should be carefully controlled in order to synthesize high-yield cubic mesoporous single crystals.

Hydrothermal treatment of as-synthesized samples is a convenient method to enlarge the pore size of mesoporous materials templated by nonionic block copolymers.[7] In the optimum reactant composition, (SI Table 1, sample A), three individual reactions were carried out at 40 °C at static conditions for 1 d, then treated differently. For the first reaction, the mixture underwent further reaction at 40 °C (SI Table 1, sample L) for 1 d. For the second reaction, the precipitates were

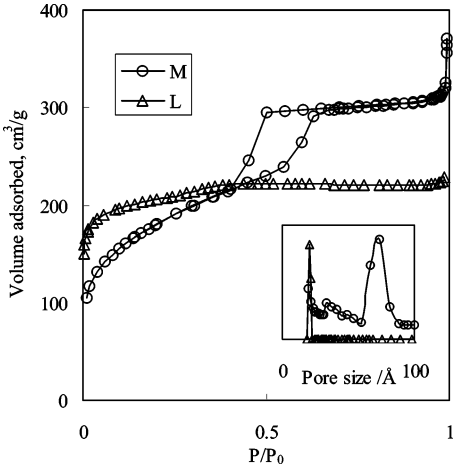

Figure 9. N_2 adsorption−desorption isotherms and pore size distribution curves (inset) of cubic mesoporous single crystals templated by F108 without and with hydrothermal treatment at 100 °C for 1 d.

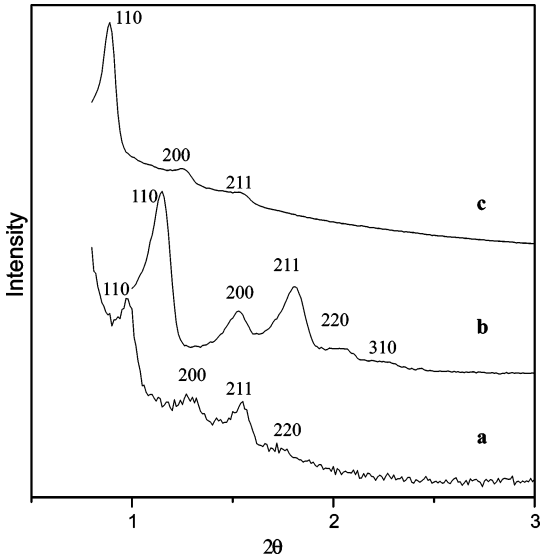

Figure 10. XRD patterns of mesoporous single crystals templated by F108 under optimum condition: (a) as-synthesized, (b) calcined samples without hydrothermal treatment, and (c) calcined samples with direct hydrothermal treatment at 100 °C for 1 d.

filtered , then 30 g of water and 0.5 g of F108 were added into a Teflon bottle together with the precipitates; such mixtures were hydrothermal treated at 100 °C for another 1 d (SI Table 1, sample M). For the third reaction, the mixtures were directly hydrothermal treated at 100 °C without filtration (SI Table 1, sample N). As-synthesized samples L and M show exclusively rhombdodecahedron shapes; calcination gives rise to little change in morphology, suggesting that the cubic macrostructure is quite stable to thermal treatments. The N_2 adsorption−desorption isotherms and pore size distribution curves calculated from the adsorption branch by BdB model of calcined samples L and M are shown in Figure 9. Both samples yield type IV sorption isotherms. Sample L without hydrothermal treatment shows no hysteresis loops; the BET surface area, pore volume, and average pore size of calcined sample L are calculated to be 698 m^2/g, 0.61 cm^3/g, and 2.1 nm (calculated by BdB model[46]), respectively. Calcined sample M hydrothermal treated at 100 °C for 1 d has a BET surface area of 670 m^2/g, a pore volume of 0.67 cm^3/g, and a mean pore size of 7.4 nm. It is interesting to note that calcined sample M shows a typical type H_2 hysteresis loop, similar to that observed in SBA-16[8] and FDU-1[47] materials with large pore, cage-like cubic structures. Hydrothermal treatment leads to significant changes in sorption isotherms and enlargement of pore sizes. Such phenomena may be related to the structure of the template F108 ($EO_{132}PO_{50}EO_{132}$). Compared to the template F127 ($EO_{106}PO_{70}EO_{106}$) used in the synthesis of SBA-16 materials, the relatively smaller weight ratio of PO groups in F108 may give rise to mesoporous materials with smaller pore sizes; and the relatively higher weight ratio of EO moieties may be responsible for the larger extent of pore size enlargement because of increasing hydrophobicity of EO (and PO) groups with temperature.[7,8,48]

If the reactant mixture were allowed to undergo hydrothermal treatment directly without filtration (SI Table 1, sample N), the morphology of resultant product is shown in Figure 8d. Some particles (2−3 μm) with polyhedral shapes are still observed, but the crystal face is less clear and smooth compared to that of sample M. More importantly, hydrothermal treatment without filtration may produce coral-like morphologies, which are composed of small spherical particles ~100−200 nm in diameter. TEM experiments reveal that such small particles possess disordered mesostructures (data not shown). XRD patterns of calcined sample N are shown in Figure 10c. For comparison, the XRD patterns of as-synthesized and calcined sample L are also listed (Figure 10, a and b, respectively). It is evident that calcined sample L possesses much higher order than calcined sample N, in accordance with the difference in their macrostructures. Obviously, the manipulation before hydrothermal treatment may greatly influence the final mesostructure and macrostructure of mesoporous materials templated by F108 copolymers.

In the synthesis of rodlike SBA-15 materials templated by P123 surfactants, the hydrothermal treatment has little influence upon the uniformity of morphology and order of mesostructure, in great contrast to what was observed in the synthesis of cubic mesoporous materials templated by F108 block copolymers (see above discussion). To understand the difference, the surfactant/Si molar ratio (R) in starting reactants and in as-synthesized samples is calculated separately for F108 and P123 templating systems (Figure 11). R in starting reactants is calculated directly and TEOS is used for the amount of Si. R in as-synthesized samples is calculated from TG analysis by using SiO_2 as the amount of Si. The weight loss of water has been taken out to obtain the weight loss of surfactants and therefore their molar amounts. The ratio of R in starting reactants versus R in as-synthesized samples is 3.4 and 1.4 for F108 and P123 templating systems, respectively. It may be deduced that in the synthesis of mesoporous materials, R in mother liquids after precipitation occurs differs from R in starting reactants and may increase with time (P123 and F108 systems). However, such variation is

(46) Lukens, W. W.; Schmidt-Winkel, P.; Zhao, D. Y.; Feng, J. L.; Stucky, G. D. *Langmuir* **1999**, *15*, 5403.
(47) Yu, C. Z.; Yu, Y. H.; Zhao, D. Y. *Chem. Commun.* **2000**, 575.
(48) Alexandridis, P.; Hatton, T. A. *Colloid Surf. A* **1995**, *96*, 1.

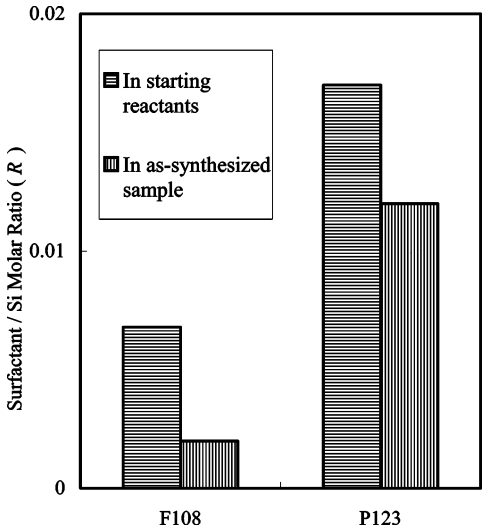

Figure 11. Surfactant/Si molar ratio (R) in starting reactants and in as-synthesized samples separately for F108 and P123 templating systems.

limited in a small range in the case of the P123 system, which may explain the fact that hydrothermal treatment does not change the mesostructure and macrostructure of SBA-15 materials since the hexagonal liquid crystal region occurs in a certain range in P123/water phase diagrams.[42] In contrast, in F108 systems, such variation is quite large and R in mother liquids after precipitation occurs may increase considerably compared to R in starting reactants. In addition, the calcined silica product yields in sample L and N are ~21 and ~90%, respectively (with respect to full conversion of SiO_2 from TEOS). In the optimum synthesis condition of cubic mesostructures by use of F108 templates, there are plenty of surfactants and silica species in solutions 1 d after precipitation occurs, and R in mother solutions should differ from R in the starting reactants and R in the precipitate to a large extent. If hydrothermal treatment is subjected to the reaction mixture without filtration (SI Table 1, sample N), the large amount of soluble surfactants and silica species in solution with significantly larger R (compared to R in starting reactants) may be responsible for the formation of disordered mesostructures with coral-like morphologies; such species may also coat onto the surface of preformed crystals, leading to polyhedral shapes with not-clear faces and enlarged particle sizes. Our results suggest that the normal hydrothermal treatment method (without filtration) may be useful in the synthesis of hexagonal mesoporous materials such as SBA-15; however, it should be carefully manipulated in the case of cubic structures.

Synthesis of Hexagonal Crystals without Salts. Inorganic salts are involved in the above synthesis of mesoporous single crystals in the presence of nonionic block copolymers and also exist in the synthetic system when cationic surfactants are employed. From the CPSM, a quick phase separation may lead to the formation of mesostructures where ΔG is dominant; therefore, synthesis condition that may quicken such phase separation may favor the formation of mesoporous single crystals. Because TMOS hydrolyzes much faster than TEOS in acidic solutions, TMOS was utilized in the synthesis of SBA-15 materials but no inorganic salts

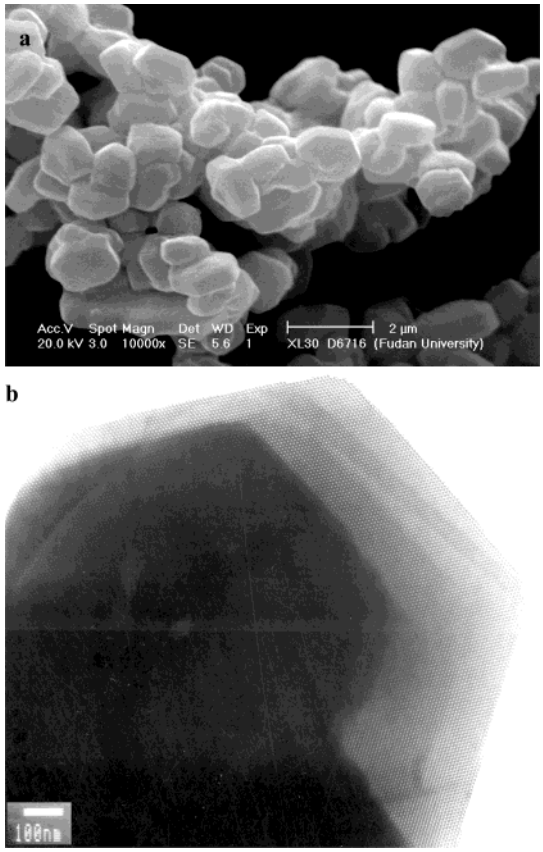

Figure 12. (a) SEM images and (b) TEM images of platelike SBA-15 materials synthesized by using TMOS as a silica source in the absence of inorganic salts.

were employed. Hexagonal platelike SBA-15 materials (1−2 μm in diameter) have been obtained (Figure 12a), and the thickness of the plates is estimated in the range of 250−500 nm. TEM images reveal that the highly ordered hexagonally arrayed channels are perpendicular to the hexagonal plane (Figure 12b); such morphology explains quite well the hexagonal mesostructure of SBA-15 materials and can be viewed as SBA-15 single crystals. It is suggested that the quick phase separation by using TMOS as a silica source is responsible for the formation of such platelike SBA-15 single crystals, in accord with the prediction of CPSM.

Size Limitation of Mesoporous Single Crystals. The definition mesoporous single crystals may be considered as a new concept compared with traditional crystals. The latter possess long-range order at the atomic scale, whereas mesoporous single crystals have repeat units at another length scale (meso-scale). Until now, the true structure of mesoporous materials has not been determined by X-ray single crystal diffraction analysis, primarily due to the limitation of particle size (usually smaller than 10 μm). Considering the mesoporous single crystals templated by block copolymers in the current study, it is interesting to note that the particle sizes are limited to ~1−2 μm despite different mesostructures (cubic or hexagonal) and synthesis conditions (with or without inorganic salts). The underlying reason is not currently understood. According to the CPSM, the mesophase is formed after phase separation and the further condensation of such liquid crystal-like phase gives rise to the final mesostructure. In this understanding, the length of micelles in liquid crystals

rather than in dilute solutions should be considered. Until now, there is no direct observation of the length of micelles in liquid crystals. By studying the self-diffusion in hexagonal lyotropic liquid crystalline phases, it is proposed that micellar rods are of finite length (a few microns);[49] such observation may be responsible for the size limitation of mesoporous single crystals and the length of mesochannels. The energy competition after phase separation may be another possible reason for such limitation: when the solid mesostructure is assembled (ΔG less negative), F may play an important role and result in morphologies toward spherical shapes in order to minimize the surface tension. It may be deduced that in order to synthesize mesoporous single crystals with large particle sizes, the influence of F should be minimized relative to the magnitude of the lattice energy of the mesostructure. In support of this conclusion, mesoporous crystals with relatively large particle sizes (2−10 μm) have been observed by using ionic surfactants as the templates,[38] because ionic surfactants usually possess lower F than block copolymers. This is also in agreement with the colloidal phase separation mechanism proposed here.

Conclusions

Synthetic conditions such as temperature, stirring rate, ionic strength, acidity, and reactants ratio that affect the mesostructures and macrostructures of mesoporous materials have been studied in a nonionic block copolymer templating system. Highly ordered SBA-15 materials with ∼100% rodlike morphologies (∼1−2 μm long) have been obtained in the presence of inorganic salts. Synthesis conditions such as low temperature, low acidity, and low ionic strength that increase the induction time give rise to morphologies with increased curvatures and decreased external surface areas. By directly observing the morphologies of particles as a function of time, a colloidal-like phase separation mechanism (CPSM) for the formation of mesoporous materials is proposed. It is suggested that the formation process of mesoporous materials involves three stages: (1) cooperative self-assembly of inorganic/organic composites; (2) formation of a new crystal-like phase rich in aggregates of block copolymer/silica species; and (3) phase separation of this liquid crystal-like phase from water and further growth of liquid crystals driven by further condensation of silica species. The morphologies of mesoporous materials are developed after the phase separation stage. Cubic ($Im\bar{3}m$) mesoporous single crystals have been obtained with exclusively rhombdodecahedron shapes (1−2 μm in size). Ultrathin microtoming TEM experiments confirm such polyhedral particles are perfect single crystals. By employing CPSM, hexagonal mesoporous single crystals (1−2 μm in diameter) have been obtained in the absence of inorganic salts. The size limitation (∼1−2 μm) of mesoporous single crystals has also been discussed. Such understandings may be useful to fabricate mesoporous materials with well-defined, crystal-like morphologies. Rodlike and platelike SBA-15 materials with variable lengths of pore channels and easily accessible mesopores may be useful for immobilization of biomolecules and for organic modification of these materials.

Acknowledgment. Supported by the National Science Foundation of China (20301004 and 20233030), State Key Research Program (01CB510202, 2002AA321010), Shanghai Science Committee (0352nm108, 03QF14002, 03DJ14004). C.Y. thanks Prof. G. D. Stucky, Colin Booth, and Prof. Paschalis Alexandridis for useful discussions.

Supporting Information Available: Table of synthetic conditions and the corresponding morpnology and induction time of mesoporous materials templated by $EO_{132}PO_{60}EO_{132}$-(F108) block copolymers (pdf). This material is available free of charge via the Internet at http://pubs.acs.org.

CM035011G

(49) Joabsson, F.; Nyden, M.; Linse, P.; Soderman, O. *J. Phys. Chem. B* **1997**, *101*, 9710.